A comparison of the full and half toroidal continuously variable transmissions in terms of dynamics of ratio variation and efficiency

A comparison of the full and half toroidal continuously variable transmissions in terms of dynamics of ratio variation and efficiency

Florian Verbelen[a,c,d], Stijn Derammelaere[a,b,d], Peter Sergeant[a,c,d], Kurt Stockman[a,c,d]

[a]*Department of Electrical Energy, Metals, Mechanical Construction and Systems, Ghent University, Belgium*
[b]*Department of Electromechanics, Op3Mech, University of Antwerp, Groenenborgerlaan 171, 2020 Antwerp, Belgium*
[c]*Member of Energy Efficient Drive Trains, www.eedt.ugent.be*
[d]*Member of Flanders Make*

Abstract

The full and half toroidal CVT have been the subject for many research papers. The efficiency and behavior in steady state of both topologies has already been discussed in detail but until now no special attention has been given to their behavior during ratio variation. Therefore, this paper discusses the comparison of the full and half toroidal CVT during periods of ratio variation focusing on the dynamic response and efficiency. The geometrical constraints for the comparison are as follows: equal output inertia, equal maximum output torque at a speed ratio of 1 and identical radial size. The results of the study are based on a model that describes the behavior of both topologies and an algorithm that determines the optimal ratio variation. The outcome of the study shows that the half toroidal outperforms the full toroidal CVT over the entire operating range in terms of dynamics and efficiency during ratio variation.

Keywords:
Continuously Variable Transmission, half toroidal, full toroidal, dynamical comparison, efficiency

1. Introduction

Manufacturers of advanced drive trains specialized in the automotive industry encounter an ever growing pressure due to increasingly stringent regulation concerning fuel consumption and emissions. As a result, they are forced to innovate and one of those innovations is the Continuously Variable Transmission (CVT). In a CVT the speed ratio can be varied continuously between two finite values. Due to their ability to vary the speed ratio in a stepless way, the CVT is used to operate the Internal Combustion Engine (ICE) of a car in its most optimal point, which results in lower fuel consumption [1, 2]. As the load conditions vary a lot due to road conditions and traffic, the speed ratio of the CVT is constantly adapted towards the optimal value in terms of efficiency of the system. This highlights the importance of a dynamic study. Besides the automotive industry, CVTs are also used in wind power systems. In those wind power systems, the gear ratio is regulated to maintain a constant generator speed in order to increase the efficiency of the system [3, 4, 5].

In literature, several types of CVT are used: toroidal CVT, belt CVT, Milner CVT [6], hydraulic CVT [7], wheel type CVT [8], ... However, the two mostly used types of variable transmissions are the belt CVT and the toroidal CVT. Belt CVTs were the first type of CVT used in mass production for automotive applications. As a result a lot of research has been done on the belt CVT. Researchers have been working on the impact of pulley deformations [9], CVT dynamics [10, 11], power losses in the belt itself [12], the effect of the control strategy on the fuel consumption in a car [13], ... Despite the advantages such as ease of implementation and control, the main drawback of the belt CVT is still the limited torque capacity and low efficiency in comparison with the toroidal CVT. Kluger [14] compared a variety of transmissions from which it is possible to conclude that the toroidal CVT has an overall efficiency which is 5.4% higher compared to the belt CVT. Imanishi [15] published a figure with the progress in torque capacity for CVTs. The current limit for the toroidal CVT is around 400 Nm while the maximum torque capacity for a belt CVT is 250 Nm. These findings are supported by Simons [16] (belt CVT 250 Nm) and Shinojima [17] (toroidal CVT 390 Nm). A solution for the rather low torque capacity of the belt CVT is provided in [18, 19] where a two stage chain CVT is presented. The maximum torque of that two stage prototype is 500 Nm.

As mentioned before, the toroidal CVT is also used in the automotive industry. There are two types of toroidal CVTs: the full and half toroidal variant (see Fig. 1). In the toroidal CVT, power is transmitted from the input disk to the output disk through a system of rollers. From the geometrical speed ratio, defined as $S_{\mathrm{rID}} = \frac{r_3}{r_1}$, it can be seen that by varying the contact points of the rollers given by the distances r_1 and r_3 respectively, the speed ratio can be varied in a continuous way. Indeed, these contact points can be changed smoothly by manipulating the tilting angle γ of the rollers. To avoid a moving contact between two metal components and the corresponding wear, a traction fluid is used.

In literature a number of modeling techniques are presented to describe the behavior of the toroidal CVT [20, 21, 22] of which this paper uses the approach of Carbone [22]. In the paper of Carbone, a detailed comparison of the steady state behavior of the full and half toroidal CVT is discussed. The conclusion of that research was that the half toroidal CVT outperforms the full toroidal over the entire operating range. Higher spin and losses due to higher slip are mentioned as the main reasons for the lower efficiency. The limitation of this analysis is that dynamic situations were neglected. However, in automotive and wind power applications, the CVT is used while the speed ratio is varied. Hence, it is important to take a closer look into those dynamic situations.

In the past, many researchers focused on the control of the speed ratio [23, 21, 24, 25] but neglected or did not discuss the relation with the efficiency during speed ratio variation. In [26], an algorithm is defined which is able to determine the optimal speed ratio variation in terms of the speed of the ratio variation (dynamics) and efficiency. The algorithm is developed for toroidal CVTs and can thus be used for both topologies. As it is the objective of this paper to compare the dynamic behavior of both variants, taking into account the efficiency during ratio variation, it is an obvious choice to use the algorithm in the comparison.

The main contribution of this work is that the dynamic behavior of both topologies is compared throughout the entire operating range. Dynamic behavior is in this paper defined as a variation in speed ratio. Efficiency variations during these dynamic events are discussed together with the

Nomenclature			
ω_{in}	input speed	n	number of rollers per unit
ω_r	roller speed	m	number of units
ω_{out}	output speed	k	aspect ratio
T_{in}	input torque	E_{eff}	effective elasticity modulus
T_{out}	output torque	$\tilde{a}_x\ \tilde{a}_y$	dimensionless semi-axes of the contact ellipse
$T_{out_{max}}$	maximum output torque	$\tilde{\tau}_{21X}\ \tilde{\tau}_{21Y}$	shear stress levels at the input
T_L	load torque	$\tilde{\tau}_{23X}\ \tilde{\tau}_{23Y}$	shear stress levels at the output
T_{BL}	bearing torque losses	$\tilde{a}_x\ \tilde{a}_y$	dimensionless semi-axes of the contact ellipse
F_N	normal force	$\mu_{in}\ \mu_{out}$	traction coefficients at input and output
$F_{N_{max}}$	maximum normal force	$\mu_{out_{max}}$	maximum output friction coefficient
ω_{spin}	spin speed	$\chi_{in}\ \chi_{out}$	spin coefficients at input and output
σ	spin ratio	p_{max}	maximum pressure
α_{in}	input acceleration	J_{out}	output inertia
S_{rID}	geometrical speed ratio	b_L	damping of the load
τ	actual speed ratio	SC	global sliding coefficient
γ	tilting angle	t_{dyn}	ratio variation period
r_1	input radius	CR	conformity ratio
r_3	output radius	$\wedge$	contact length parameter
θ	half cone-angle	η_ω	speed efficiency
e_d	eccentricity	η_T	torque efficiency
r_{22}	roller curvature	η	efficiency
r_0	cavity radius	$M_{S_{in}}\ M_{S_{out}}$	spin momentum at input and output
r_2	roller radius	$F_{T_{in}}\ F_{T_{out}}$	traction force at input and output
J_r	roller inertia	$J_{r,out}$	inertia of a single output disc

time taken to vary the speed ratio over a predefined step. As a result of this study, some design guidelines, independent of the technology, are presented which have an impact on the dynamic behavior of the CVT.

This paper is structured as follows. Section 2 discusses the geometrical differences between both toroidal topologies. The model and the optimal ratio variation algorithm are briefly reviewed in, respectively section 3 and 4. Section 5 describes the differences in torque capacity between the full and half toroidal CVT. In section 6 the differences in dynamics are discussed while in section 7 the differences in efficiency during ratio variation are considered. The design guidelines are introduced in section 8. In section 9 additional dynamic results are given to validate the considered figures and finally in section 10 the conclusions of the research are formulated.

2. Geometrical differences between half and full toroidal CVT

In this section the geometrical differences between the half and full toroidal CVT are highlighted. The geometrical structure of the half and full toroidal CVT is displayed in, respectively Fig. 1 a) and b). Both topologies are clearly very similar and can therefore be defined by the same set of geometrical parameters. The values given to these parameters can be found in Table 1 [22].

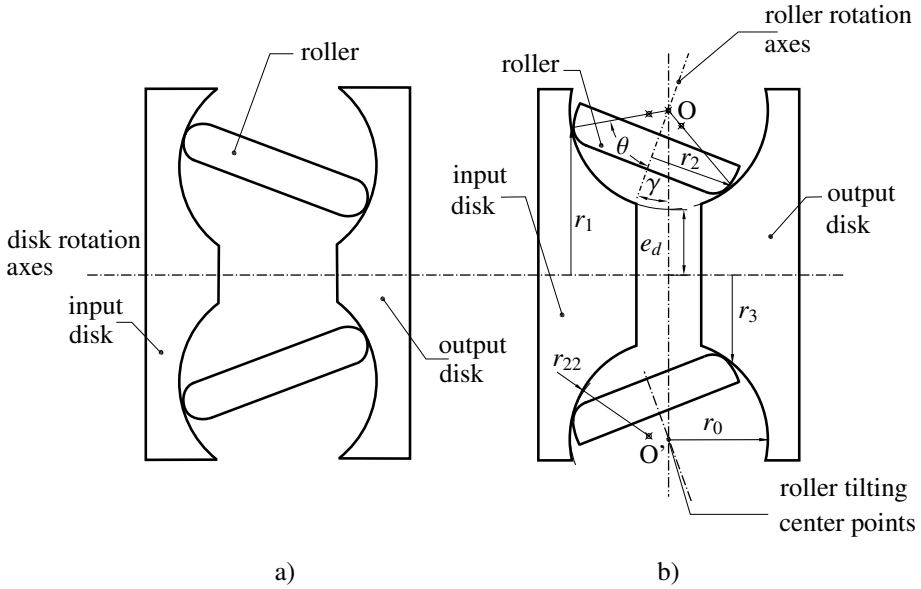

Figure 1: a) Full toroidal CVT; b) Half toroidal CVT.

Table 1: CVT geometric data

Full toroidal CVT:	Half toroidal CVT:
Cavity radius $r_0 = 40$ mm	Cavity radius $r_0 = 40$ mm
Conformity ratio $CR = \frac{r_{22}}{r_0} = 0.67$	Conformity ratio $CR = \frac{r_{22}}{r_0} = 0.8$
Half cone-angle $\theta = \frac{\pi}{2}$ rad	Half cone-angle $\theta = \frac{\pi}{3}$ rad
Aspect ratio $k = \frac{e_d}{r_0} = 0.25$	Aspect ratio $k = \frac{e_d}{r_0} = 0.625$
Number of rollers per unit $n = 3$	Number of rollers per unit $n = 3$
Number of units $m = 1$	Number of units $m = 1$
Speed ratio range $\tau = 0.5 - 2$	Speed ratio range $\tau = 0.5 - 2$

The parameter which identifies a toroidal CVT as the half or full variant is the half cone-angle θ. In [27] the full toroidal CVT was defined as a toroidal CVT with a half cone-angle of $\frac{\pi}{2}$ rad. Later many authors followed that definition [22, 28, 29]. The advantage of a half cone-angle of $\frac{\pi}{2}$ rad is that the normal forces on the roller are balanced out. Therefore there is no resulting axial force on the rollers and consequently no axial bearing is necessary. For the half toroidal CVT, the half cone-angle is less strictly defined and varies around $\frac{\pi}{3}$ rad [30, 25, 22, 31, 32, 33]. A half cone-angle between $\frac{\pi}{3}$ and $\frac{\pi}{2}$ rad is not interesting as this type of CVT does not benefit from the steep traction curve of a half toroidal CVT nor will it benefit from low bearing losses in the rollers due to zero axial force.

Another rather striking difference between both CVTs is the aspect ratio k. The aspect ratio k is defined as the ratio of the eccentricity e_d and the cavity ratio r_0 (see Fig. 1). Unlike the half cone-angle this difference is not based on a definition but on a constraint. In this paper the cavity radius and the radial size of both CVTs are chosen to be identical. This constraint can only be

fulfilled when both CVTs have a different aspect ratio [22]. The radial size is chosen to be the same for both technologies as it has an impact on the torque capacity which has a large impact on the dynamics as will be shown later on.

The last difference between both CVTs is the conformity ratio *CR* which is defined as the ratio of the roller curvature r_{22} and the cavity radius r_0. The reasoning behind the chosen value for *CR* is given in section 5.2.

3. Model of the toroidal CVT

In the previous section it was shown that both CVTs have the same structure which is defined by parameters such as the half cone-angle and conformity ratio. The difference between the half and full toroidal CVT model is merely in the values of those parameters. As a consequence, the same model can be used to simulate the behavior of both topologies. The model which is used in this paper has been derived in [26] and is based on [22]. The model which is validated based on multiple publications as stated in [26], is briefly summarized in this section.

The structure of the model is shown in Fig. 2. All variables are defined in the nomenclature table. The model of the toroidal CVT consists of a mechanical and a contact model which are both described in the next paragraphs. Furthermore, it contains a simple load model.

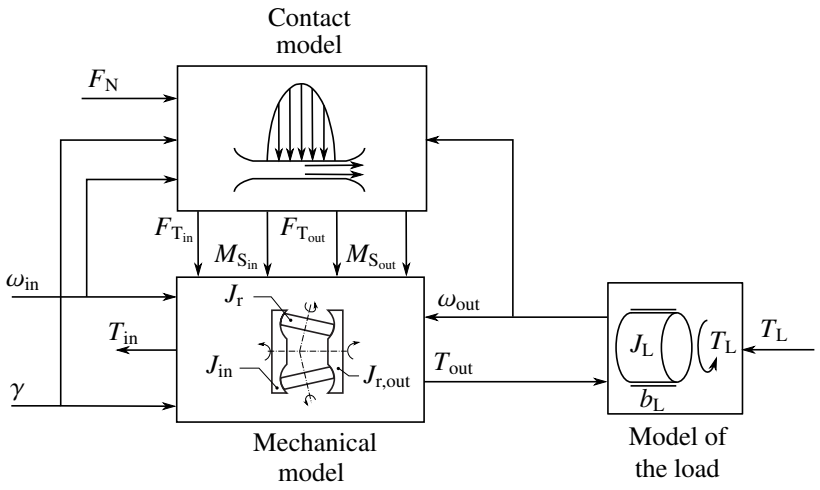

Figure 2: Model structure of the half toroidal CVT

For the mechanical model, shown in Fig. 2, the dynamic equations of the complete CVT are given in eq. (1) and are written based on the free body diagram visualized in Fig. 3. In the upper equation, speed of the input disc is an input variable. This means that the dynamics of the input disc are not considered. Note that $\frac{d\gamma}{dt}$ is ignored in the middle equation due to its small impact.

T_{BL} stands for the bearing losses and depends on the considered topology. In a half toroidal CVT there is both an axial and radial force component on the rollers. Therefore, a combination

of axial thrust and needle bearings are used to support the rollers [30, 31, 34]. This bearing combination is not necessary for the full toroidal CVT as the axial forces are balanced out. As a result only the needle bearings are necessary to support the rollers [31]. The models which are used to calculate the torque losses in the bearing combinations are based on the equations and data provided by SKF [35]. A similar method to model the bearing losses in toroidal CVTs has been used in [29, 31, 36]. The impact of both speed and axial/radial force on the losses are incorporated.

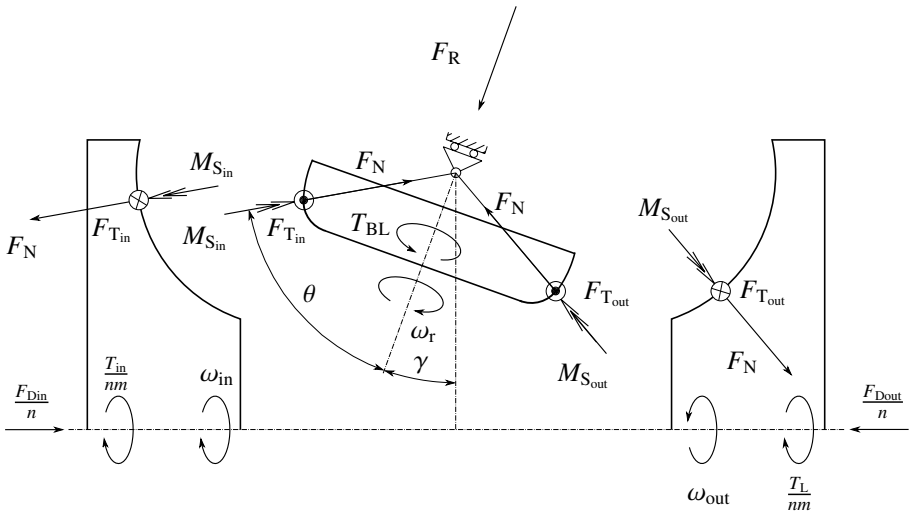

Figure 3: Free body diagram of half toroidal CVT. The symbol $\bigotimes$ is used for vectors pointing away from the reader. The symbol $\odot$ is used for vectors pointing towards the reader.

$$\begin{cases} T_{\text{in}} & = m\,n\,\mu_{\text{in}} F_{\text{N}} r_1 + m\,n\,\chi_{\text{in}} F_{\text{N}} r_1 \sin(\theta+\gamma) \\ J_{\text{r}} \frac{d\omega_{\text{r}}}{dt} & = \mu_{\text{in}} F_{\text{N}} r_2 + \chi_{\text{in}} F_{\text{N}} r_1 \cos(\theta) - \mu_{\text{out}} F_{\text{N}} r_2 + \chi_{\text{out}} F_{\text{N}} r_3 \cos(\theta) - T_{\text{BL}} \\ m J_{\text{r,out}} \frac{d\omega_{\text{out}}}{dt} & = m\,n\,\mu_{\text{out}} F_{\text{N}} r_3 - m\,n\,\chi_{\text{out}} F_{\text{N}} r_3 \sin(\theta-\gamma) - T_{\text{L}} \end{cases} \tag{1}$$

The contact model used in this paper was originally presented in [22]. Carbone adapted a model for fully flooded isothermal contacts to evaluate slip and spin losses. In the model, the pressure distribution is calculated according to Hertz law. This assumption is generally accepted in hard-EHL contact as the fluid film thickness of the oil is almost constant at high contact pressures [22, 37]. Once the pressure distribution is known, the viscosity of the traction fluid can be determined throughout the contact area. Through viscosity, film thickness is calculated by which it is possible to determine the shear stress levels in the fluid film. The fluid properties can be found in [26]. The last step in the contact model is to calculate the traction coefficients μ and the spin momentum values χ. This is done by solving the integrals in eq. (2)-(5).

$$\mu_{\text{in}} = \tilde{a}_{\text{X}_{\text{in}}}\tilde{a}_{\text{Y}_{\text{in}}}\int_0^1\int_0^{2\pi}\tilde{\tau}_{21\text{X}}Rd\psi dR \tag{2}$$

$$\mu_{\text{out}} = -\tilde{a}_{\text{X}_{\text{out}}}\tilde{a}_{\text{Y}_{\text{out}}}\int_0^1\int_0^{2\pi}\tilde{\tau}_{23\text{X}}Rd\psi dR \tag{3}$$

$$\chi_{\text{in}} = \frac{\tilde{a}_{\text{X}_{\text{in}}}\tilde{a}_{\text{Y}_{\text{in}}}\wedge}{r_0\tilde{r}_1}\int_0^1\int_0^{2\pi}\left(\tilde{a}_{\text{X}_{\text{in}}}\tilde{\tau}_{21\text{Y}}\cos\psi - \tilde{a}_{\text{Y}_{\text{in}}}\tilde{\tau}_{21\text{X}}\sin\psi\right)R^2 d\psi dR \tag{4}$$

$$\chi_{\text{out}} = \frac{\tilde{a}_{\text{X}_{\text{out}}}\tilde{a}_{\text{Y}_{\text{out}}}\wedge}{r_0\tilde{r}_3}\int_0^1\int_0^{2\pi}\left(\tilde{a}_{\text{X}_{\text{out}}}\tilde{\tau}_{23\text{Y}}\cos\psi - \tilde{a}_{\text{Y}_{\text{out}}}\tilde{\tau}_{23\text{X}}\sin\psi\right)R^2 d\psi dR \tag{5}$$

where μ_{in} and μ_{out} are the traction coefficients between input & roller and roller & output respectively. The spin coefficients between the contacts are given by χ_{in} and χ_{out}. The shear stress levels at input and output are defined as $\tilde{\tau}_{21\text{X}}$,$\tilde{\tau}_{21\text{Y}}$,$\tilde{\tau}_{23\text{X}}$ and $\tilde{\tau}_{23\text{Y}}$. The dimensionless semi-axis of the contact ellipses are represented by $\tilde{a}_{\text{X}}$ and $\tilde{a}_{\text{Y}}$. R and ψ are the result of the following coordinate transformation:

$$\begin{cases} X = R\cos(\psi) \\ Y = R\sin(\psi) \end{cases} \tag{6}$$

with $0 \leq R \leq 1$ and $0 \leq \psi \leq 2\pi$.

4. Optimal ratio variation algorithm

As mentioned in the introduction, the optimal ratio variation algorithm defined in [26] will be used to compare the ratio variation characteristics of both topologies. The main idea behind the algorithm is to control the output torque of the CVT during ratio variation in such a way that it never exceeds its maximum value. The advantage of this methodology is that the increase in slip is minimized and the fastest possible speed ratio variation is obtained [26]. Because of these properties, the algorithm is ideal to examine the differences in dynamics of the full and half toroidal CVT.

The first step of the procedure, which is summarized in Fig. 4, is to calculate the optimal speed ratio τ^* by solving eq. (7) which has been derived in [26]. It is important to mention that the output inertia J_{out} in this equation considers both the inertia of the output discs of the CVT $J_{\text{r,out}}$ as the inertia of the load J_{L}.

$$\frac{\text{d}\omega_{\text{in}}}{\text{d}t}\left\{\tau^*(\gamma)\right\}_{\max} + \omega_{in}\left\{\frac{\text{d}\tau^*(\gamma)}{\text{d}t}\right\}_{\max} = \frac{T_{\text{out}_{\max}} - T_{\text{L}}}{J_{\text{out}}} \tag{7}$$

As the used model is driven by the tilting angle γ (see Fig. 2) and the solution of eq. (7) is denoted as speed ratio $\tau^* = \frac{\omega_{\text{out}}}{\omega_{\text{in}}}$, the tilting angle has to be calculated based on eq. (8):

$$\gamma = -2\arctan\left\{\frac{-(\tau^*+1)\sin(\theta) + \sqrt{(\tau^*+1)^2\sin^2(\theta) - \left[(\tau^*-1)(k+1)\right]^2 + \left[(\tau^*-1)\cos(\theta)\right]^2}}{(\tau^*-1)\left[(k+1)+\cos(\theta)\right]}\right\} \tag{8}$$

The optimal path for the tilting angle can now be found by solving these equations iteratively until the final desired speed ratio value is obtained. In eq. (7), the maximum output torque $T_{\text{out}_{\text{max}}}$ has a significant impact on the optimal tilting angle. Parameters such as the load torque and input speed can be considered as input parameters while the output inertia is a constant, geometrical parameter, defined in the design stage. When both CVTs will be compared the input and geometrical parameters will be kept the same for comparative simulations. Therefore differences in the output torque of both CVTs will result in differences in dynamics. The maximum output torque of a toroidal CVT is defined as [26]:

$$T_{\text{out}_{\text{max}}} = m\, n\, F_{\text{N}_{\text{max}}} \mu_{\text{out}_{\text{max}}} r_3 \tag{9}$$

Eq. (9) indicates that the maximum output torque is determined by the total number of rollers mn, the maximum normal force $F_{\text{N}_{\text{max}}}$, the maximum friction coefficient $\mu_{\text{out}_{\text{max}}}$ and the distance between the contact point at the output and the center line of the output disk r_3. The presence of r_3 indicates that the maximum output torque depends on the tilting angle and thus on the speed ratio.

Besides the speed ratio, the maximum normal force $F_{\text{N}_{\text{max}}}$ has an impact on the maximum output torque. This maximum normal force is determined by the maximum pressure which is defined at the design phase of the CVT. Modern CVTs are designed in order to withstand pressures up to 3GPa [38, 22, 39]. The relationship between force and pressure can be written as [26]:

$$\tilde{p}_{\text{max}} = \frac{3}{2} \frac{1}{\pi \tilde{a}_{\text{x}} \tilde{a}_{\text{y}}} = \frac{p_{\text{max}} \wedge^2}{F_{\text{N}}} \tag{10}$$

Which can be redrafted as:

$$F_{\text{N}} = \frac{2}{3} \pi \tilde{a}_{\text{x}} \tilde{a}_{\text{y}} \wedge^2 p_{\text{max}} \tag{11}$$

In eq. (11), the contact length parameter $\wedge$ is equal to [22]:

$$\wedge = \left(\frac{6 F_{\text{N}} r_0}{\pi E_{\text{eff}}} \right)^{\frac{1}{3}} \tag{12}$$

Which can be used to rewrite eq. (11) in final form as:

$$F_{\text{N}_{\text{max}}} = \frac{32}{3} \pi r_0^2 p_{\text{max}}^3 \tilde{a_x}^3 \tilde{a_y}^3 \frac{1}{E_{\text{eff}}^2} \tag{13}$$

For further details considering the parameters in eq. (13), consider [26]. From eq. (13) it is clear that the maximum pressure p_{max} has an important impact on the dynamics. If that maximum pressure is increased due to design modifications or improved performance of the used traction fluid, the maximum normal force will increase. Because maximum normal force defines maximum torque, pressure will thus have a significant impact on the dynamics of the CVT. Therefore

it is very important that the maximum pressure is kept the same for both CVTs in order to have a fair comparison.

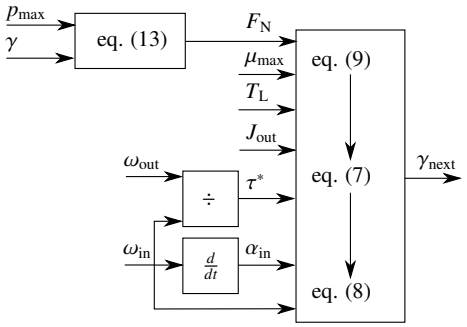

Figure 4: Work flow and required inputs for the proposed procedure.

5. Differences in torque capacity

The output torque T_{out} plays a significant role on the dynamics of the CVT. Therefore it is vital to understand what influences the maximum torque $T_{out_{max}}$ for both CVTs. If both topologies are compared based on eq. (9), the following parameters can be eliminated as they are the same for each variant: m, n and r_3. Therefore, any difference in torque capacity will be due to differences in maximum friction coefficient $\mu_{out_{max}}$ or maximum normal force $F_{N_{max}}$.

5.1. Maximum friction coefficient $\mu_{out_{max}}$

The maximum friction coefficient can be studied based on the traction curve which describes the relation between the friction coefficient and the global sliding coefficient SC which is also know as creep [22] or slip. From this relation, shown in Fig. 5, it is possible to observe that there is no significant difference between the maximum value of the friction coefficient for both topologies. This makes sense as the maximum friction or traction coefficient highly depends on the chosen traction fluid [40, 41] which is the same for both topologies. What is striking, as also being pointed out in [22, 31, 29], is the value for the global sliding coefficient at which these maximum values are reached. The full toroidal CVT will reach its maximum friction coefficient and thus optimal traction capabilities at much higher values of the global sliding coefficient which means that it will operate at much lower speed efficiency values ($\eta_\omega = 1 - SC$). As the optimal ratio variation algorithm aims for the maximum output torque and thus maximum friction coefficient, it can be expected that efficiency during ratio variation will be lower for the full toroidal than the half toroidal CVT as slip will increase more.

The differences in the traction curves of both topologies can be explained based on spin. Spin is a parasitic effect which has its origin in the geometry of the roller and toroidal cavity [31]. The spin velocity of the input disk can be written as follows:

$$\omega_{spin} = \omega_{in} \sin(\theta + \gamma) - \omega_r \cos(\theta) \tag{14}$$

The dimensionless form of spin is the spin ratio σ which indicates how much the CVT suffers from spin. If slip is neglected the following equation for the spin ratio σ between input and intermediate roller can be deduced [22]:

$$\sigma = \frac{\omega_{\text{spin}}}{\omega_{\text{in}}} = \frac{\cos\gamma - (1+k)\cos\theta}{\sin\theta} \tag{15}$$

From eq. (15) it is easily seen that the spin coefficient σ will always be smaller for the half toroidal CVT as the aspect ratio k for the half toroidal CVT is bigger than for the full toroidal variant. This means that the full toroidal CVT is much more affected by spin motion. As spin motion causes energy dissipation and a reduction in traction capabilities, it should be reduced as much as possible. The higher the spin motion, the more creep (higher value for SC) is necessary to transmit a certain amount of torque. As torque can be translated to a friction coefficient, under the assumption of constant normal force, a default friction coefficient will be reached at higher creep values for the full toroidal CVT. Hence, the difference in traction curve will predominantly have an impact on the torque generation during dynamic situations while SC is varying.

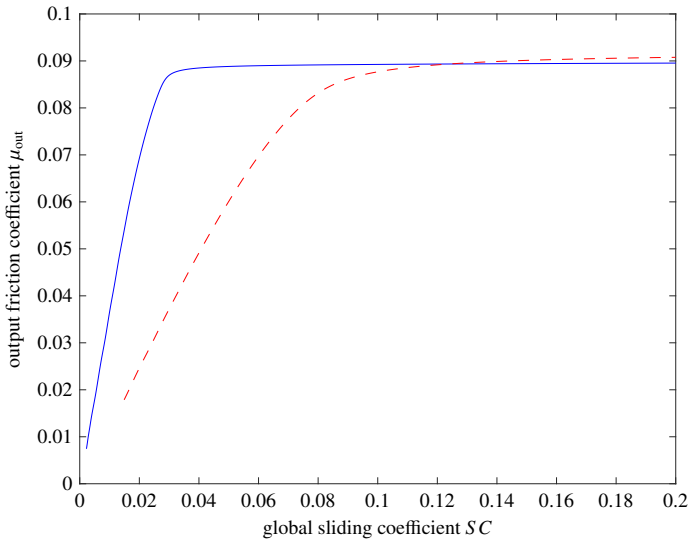

Figure 5: Friction coefficient at the output μ_{out} as function of global sliding coefficient SC. Speed ratio τ is equal to one and the maximum pressure is kept constant at 2.5GPa. Blue, full line: half toroidal. Red, dashed line: full toroidal.

5.2. Maximum normal force $F_{\text{N}_{\text{max}}}$

The second parameter which is discussed is the maximum normal force $F_{\text{N}_{\text{max}}}$ on the contact. To get a first impression of the differences between both topologies, a comparison has been made between the half toroidal CVT as presented in Table 1 and full toroidal CVT based on an optimal parameter set as defined in [28]. This intermediate step is necessary to understand the reasoning behind the chosen geometrical parameters for the full toroidal CVT which are listed in Table 1.

The results of this intermediate comparison are shown in Fig. 6. The figure shows a compelling difference in maximum normal force between both technologies. In this case the torque capacity of the half toroidal CVT will be twice as big as the torque capacity of the full toroidal CVT. However, this does not mean that the optimal parameter set produced by Delkhosh in [28] is wrong as Delkhosh searched for a parameter set which would result in a full toroidal CVT with the highest efficiency.

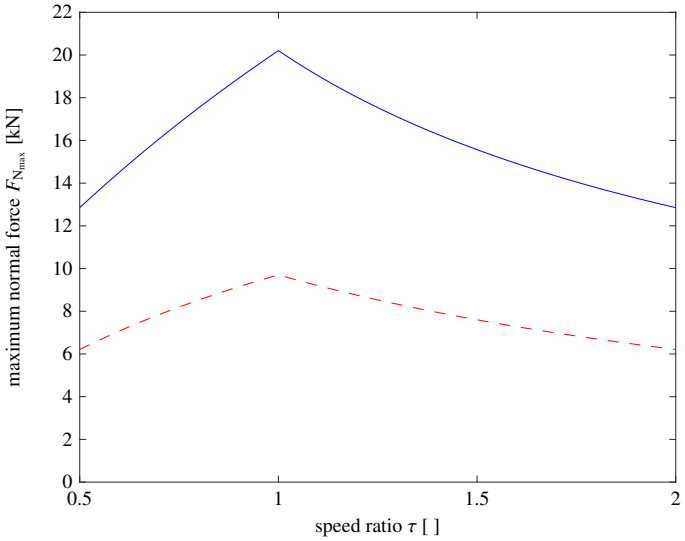

Figure 6: Maximum normal force $F_{N_{max}}$ as function of speed ratio τ, based on the geometrical data listed in Table 1 with the conformity ratio of the full toroidal CVT as exception ($CR = 0.5$). Results valid for a maximum pressure of 2.5 GPa. Blue, full line: half toroidal. Red, dashed line: full toroidal.

In order to understand what lies at the origin of this difference it is important to know which parameter has an impact on both torque capacity and efficiency. That parameter is the conformity ratio CR. The optimal value, in terms of efficiency, is 0.5 according to [28]. This is confirmed by Fig. 7. In this figure simulations are performed based on full toroidal CVTs with different CR values. The figure clearly shows that for a value of 0.5 the efficiency is maximal. Higher values of CR are penalized with a lower maximum efficiency but what is striking is the maximum torque which is reached. For increasing CR, the maximum output torque is also increasing. This means that the price to pay for efficiency optimization by constraining CR to 0.5 is a limited torque capacity.

This phenomenon can be explained with Fig. 8. Given a maximum pressure, which is defined at the design stage of the CVT, a certain maximum normal force can be calculated. As can be seen in Fig. 8, the maximum normal force increases when the conformity ratio increases (for a fixed contact pressure) and from eq. (9) it is known that if the maximum normal force increases the maximum output torque will also increase. This makes sense as a larger conformity ratio will result in a bigger contact area and thus a higher force can be applied to obtain a certain pressure.

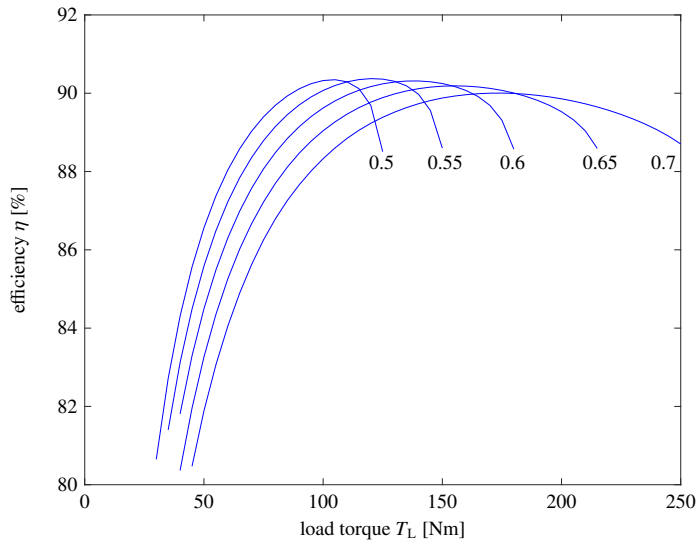

Figure 7: Efficiency η as function of load torque T_L for conformity ratio CR between 0.5 and 0.7. Speed ratio τ is equal to one and the maximum pressure is kept constant at 2.5GPa.

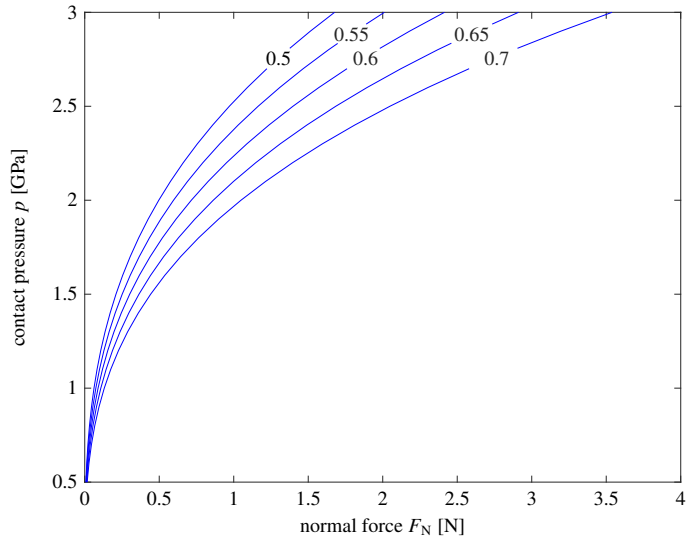

Figure 8: Contact pressure p as function of normal force F_N for conformity ratio CR between 0.5 and 0.7. Speed ratio τ is equal to one.

The previous figures were based on a fixed speed ratio. By varying the speed ratio throughout the simulations the torque capacity can be determined throughout the operating area. Fig. 9 gives

an overview of the impact of the conformity ratio and the speed ratio on the maximum output torque of the full toroidal CVT.

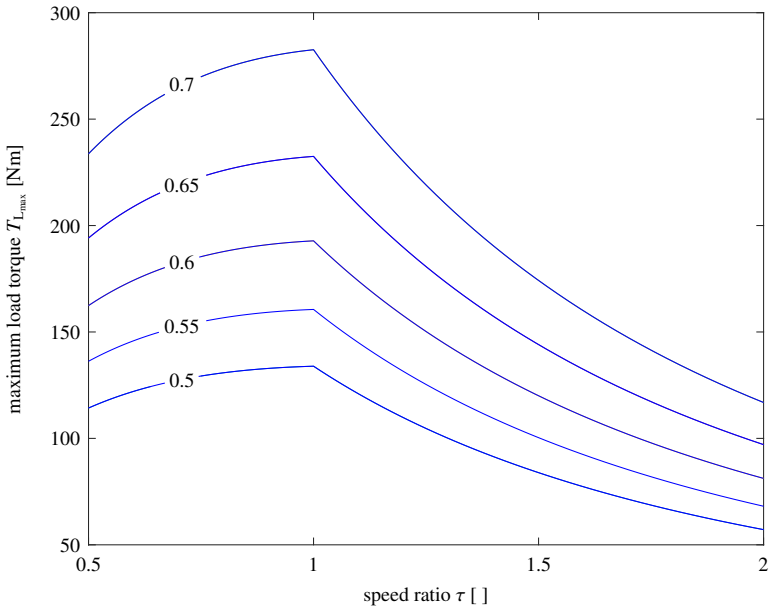

Figure 9: Maximum load torque $T_{L_{max}}$ as function of speed ratio τ for conformity ratio CR between 0.5 and 0.7 at a maximum pressure of 2.5 GPa.

What is noticeable in Fig. 9 is the negative effect of high and low speed ratio values on the maximum output torque. This effect is clearly visible when the maximum output torques of the half and full toroidal CVT are compared (see Fig. 10). In this comparison the conformity ratio has been adapted in such a way that the maximum output torque at a speed ratio of 1 would be the same for both CVTs. The fact that there is a clear difference in output torque means that there will be a difference in dynamics.

To validate the curves of the maximum output torque, simulations have been performed throughout the entire operating range of both CVTs. The load torque was increased until an unstable condition (gross slip) occurred. The previous load torque (stable operation) was than plotted in Fig. 10 as the $*$. The considered CVTs in Fig. 10 are modeled based on the geometrical data listed in Table 1.

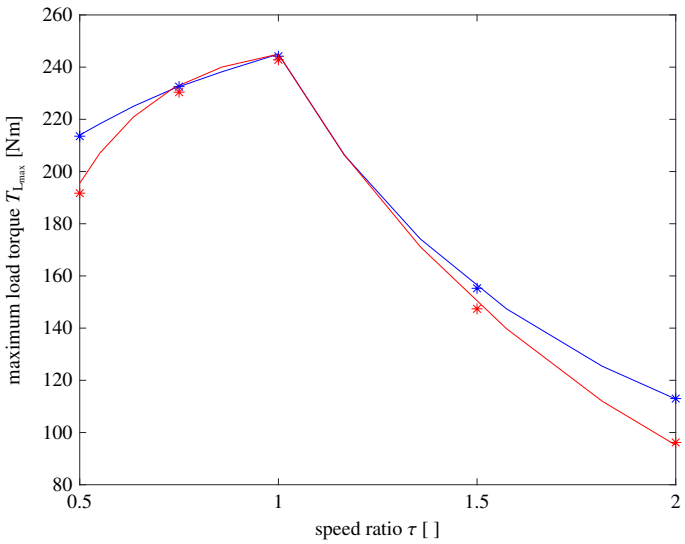

Figure 10: Maximum load torque $T_{L_{max}}$ of the half toroidal (blue) and full toroidal (red) CVT as function of speed ratio τ. The continuous lines represent the solution of eq. (9) while the $*$ represent the values obtained in simulation. CVTs modeled based on geometrical data listed in Table 1.

6. Differences in dynamics

To compare the dynamics, the process of ratio variation has been monitored for a delta in speed ratio of 0.1 throughout the operating range. To this end, the optimal ratio variation algorithm (see Fig. 4) is used to calculate the optimal path of the tilting angle from the initial speed ratio τ_0 until the final speed ratio $\tau_0 \pm 0.1$ (acceleration and deceleration). This predefined delta value has been chosen based on Fig. 11. The figure shows the response of the half toroidal CVT during ratio variation for two different delta values: 0.025 (red curve) and 0.1 (blue curve). What should be noticed is that the maximum output torque is not immediately achieved. The delta value is thus selected such that the maximum output torque is achieved before or at the end of the ratio variation process. This phenomenon is due to the fact that the output inertia J_{out} needs to be accelerated which takes some time and limits the dynamics. This J_{out} is chosen to be 0.1 kgm^2 for both topologies. In this value for J_{out}, both the inertia of the output disc $J_{r,out}$ and a load inertia J_L have been considered in order to achieve more realistic values for the ratio variation period.

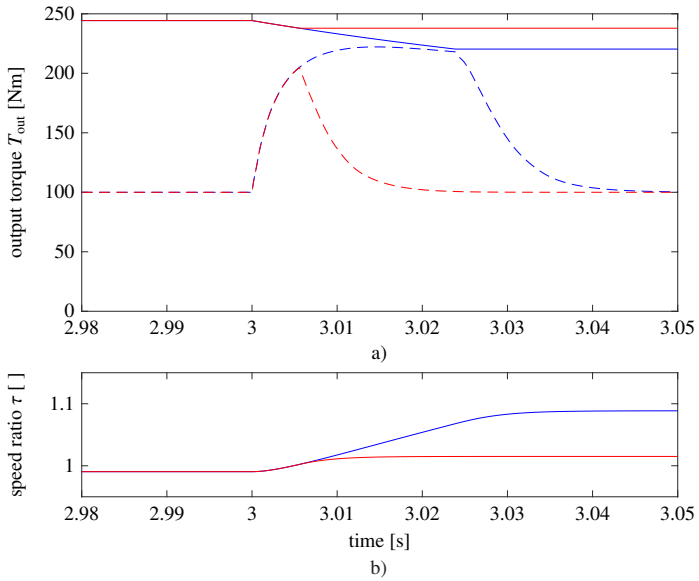

Figure 11: a) Maximum output torque $T_{\text{out}_{\text{max}}}$ (full line) and actual output torque T_{out} (dashed line) for a delta in speed ratio of 0.1 (blue curve) and 0.025 (red curve). b) Speed ratio τ for a delta in speed ratio of 0.1 (blue curve) and 0.025 (red curve).

Fig. 12 displays the time needed for the half toroidal CVT to vary the speed ratio over the default value of 0.1 as function of speed ratio in case of acceleration (continuous line) and deceleration (dashed line). The different colors represent speed ratio variations for different load torque T_{L}. The green line, for example, shows the dynamic behavior at a load torque of 150 Nm.

The optimal path of the tilting angle is calculated based on eq. (7). This equation shows that the difference between the maximum output torque and the actual torque is inversely proportional with the ratio variation period ($T_{\text{out}_{\text{max}}} - T_{\text{L}} \sim \frac{1}{t_{\text{dyn}}}$). This can also be deduced from Fig. 12. Take for example the acceleration phase (continuous lines) and a speed ratio τ of 1, then the maximum output torque $T_{\text{out}_{\text{max}}}$ for all considered points is the same. As the blue line $T_{\text{L,blue}}$ corresponds with the lowest load torque, $T_{\text{out}_{\text{max}}} - T_{\text{L}}$ is largest for the blue line. Therefore, the ratio variation period of the blue line is expected to be the shortest which is confirmed by Fig. 12.

This inversely proportional relation is also observable at the boundaries of the curves. When the difference between torque capacity and load torque becomes small, the period of ratio variation soars to extremely high values. Some curves are limited to a certain speed ratio as the load torque becomes higher than the torque capacity (black curve).

Considering a comparison between the acceleration and deceleration phase it is possible to say that the ratio variation period of the deceleration phase is shorter over the entire operating range than the acceleration phase (see Fig. 12). This makes sense as in the deceleration phase, the load torque actively decelerates the output. The larger this active component, the bigger the difference between acceleration and deceleration (black line in comparison with blue line). Besides this

difference the deceleration phase follows the same trend as the acceleration phase. Therefore, for the remainder of the paper, only the acceleration phase will be further discussed.

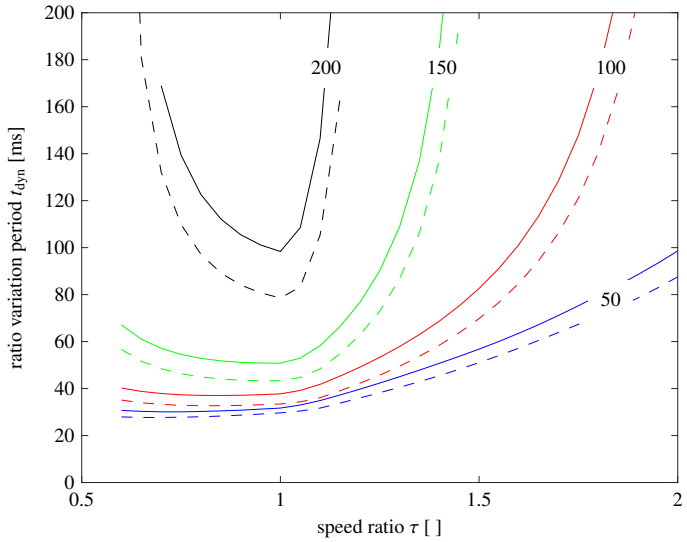

Figure 12: Ratio variation period t_{dyn} [ms] of the half toroidal CVT as function of speed ratio values τ between 0.6 and 2 for load torque values T_L between 50 and 200 Nm. The continuous lines represent the acceleration phase while the dashed lines represent the deceleration phase.

To compare the dynamics of both topologies, the half toroidal CVT is used as reference. The difference in dynamics is plotted as a percentage difference where 0% stands for an equal ratio variation period. The results are shown in Fig. 13. From this figure it is easy to deduce that the half toroidal outperforms the full toroidal over the entire operating range. The difference becomes bigger for increasing speed ratio. This is something which could be expected based on Fig. 10. As speed ratio increases, the difference between the torque capacity increases which results in larger differences in ratio variation period.

Despite the proven link between torque capacity and ratio variation period, some deviations from what could be expected are noticeable. Between a speed ratio of 0.75 and 1.2 the maximum output torque of the full toroidal CVT is equal or slightly higher than the maximum output torque of the half toroidal CVT (see Fig. 10). Based on this information, one could expect a shorter ratio variation period in that region of speed ratio values. Fig. 13 shows that this is not the case and the reason for it is the difference in slip (global sliding coefficient or creep). As shown on the traction curve (see Fig. 5), both CVTs will operate at entirely different values for slip if the maximum output torque is required. In case of the full toroidal CVT this means much higher slip levels which increase even more during ratio variation. The higher the variations in slip, the longer it takes before slip reaches its steady state value which is a disadvantage for the full toroidal CVT. This drawback explains why the full toroidal is slower even in the area where its maximum torque overcomes the maximum torque of the half toroidal CVT.

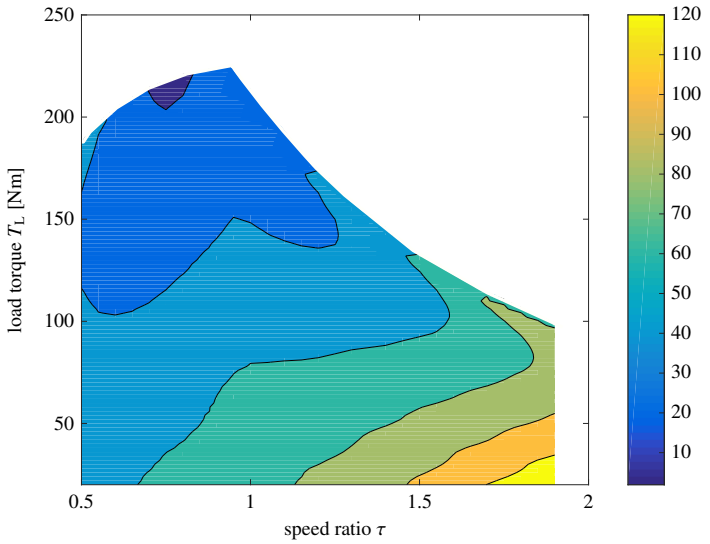

Figure 13: Difference in ratio variation period $\frac{t_{\text{dyn,full}} - t_{\text{dyn,half}}}{t_{\text{dyn,half}}}$ [%] between half and full toroidal CVT.

7. Differences in efficiency during ratio variation

As mentioned in section 6, slip will increase much more during ratio variation for the full toroidal CVT than for the half toroidal CVT. This statement is confirmed by Fig. 14 where it can be observed that not only the steady state values for the slip are much higher for the full toroidal compared to the half toroidal CVT but also the peak values during ratio variation.

The figure also shows the impact of the load torque on the slip. As the load torque increases, slip reaches higher peak values during ratio variation. While slip variations during ratio variation are limited to 1-2% for the half toroidal CVT, this number is up to 3 times bigger for the full toroidal CVT. This also means that the torque capacity during ratio variation will be influenced much more for the full toroidal CVT than for the half toroidal CVT as gross slip will occur much faster. This can be observed on Fig. 15 where there is a clear difference in maximum output torque during ratio variation although they have the same steady state torque capacity as shown in Fig. 10.

To calculate the efficiency in dynamic situations, the instantaneous power at the input and output are used:

$$\eta = \frac{P_{\text{out}}}{P_{\text{in}}} = \frac{\omega_{\text{out}} T_{\text{out}}}{\omega_{\text{in}} T_{\text{in}}} \tag{16}$$

in which, according to [22], the input and output torque can be written in terms of traction coefficients as follows:

$$T_{\text{in}} = mnF_{\text{N}}r_1\left(\mu_{\text{in}} - \chi_{\text{in}}\sin\left(\theta+\gamma\right)\right) \tag{17}$$

$$T_{\text{out}} = mnF_{\text{N}}r_3\left(\mu_{\text{out}} - \chi_{\text{out}}\sin\left(\theta-\gamma\right)\right) \tag{18}$$

leading to the following equation for the efficiency:

$$\eta = \frac{\omega_{\text{out}}\left(\mu_{\text{out}} - \chi_{\text{out}}\sin\left(\theta-\gamma\right)\right)r_3}{\omega_{\text{in}}\left(\mu_{\text{in}} + \chi_{\text{in}}\sin\left(\theta+\gamma\right)\right)r_1} \tag{19}$$

To synthesize the efficiency in one value during dynamic situations, the average efficiency during the period of ratio variation is calculated. The period is fixed for each operating point and is defined by the period of ratio variation of the full toroidal CVT. The 2 main reason for this are: the period over which the average is calculated has to be the same for both topologies and the period of ratio variation for the full toroidal CVT is always longer. The efficiency values during ratio variation can be found in Fig. 15 a) and b).

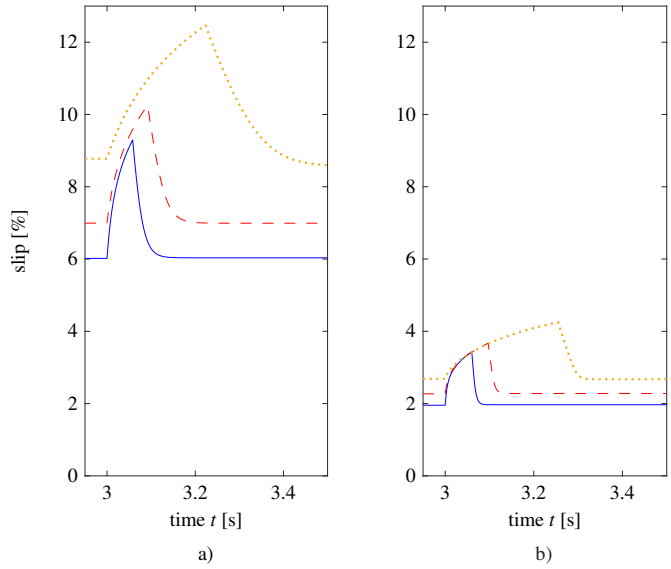

Figure 14: Slip during ratio variation as function of time for different values of load torque T_{L}. a) Full toroidal CVT. b) Half toroidal CVT. Blue, full line: 190 Nm. Red, dashed line: 210 Nm. Orange, dotted line: 230 Nm.

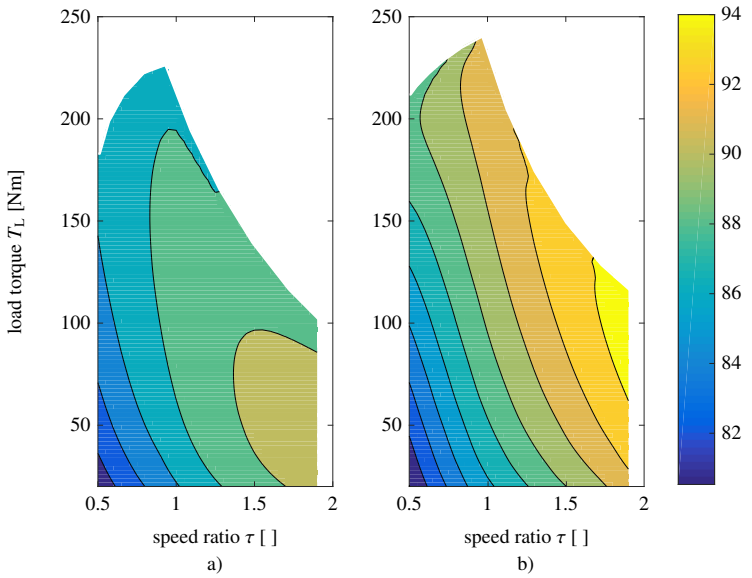

Figure 15: Comparison of the efficiency [%] during ratio variation of the toroidal CVT as function of the load torque T_L and the speed ratio τ. a) Full toroidal CVT. b) Half toroidal CVT.

To actually compare the efficiency of both technologies during ratio variation, the difference of both maps is presented in Fig. 16. This figure shows that the half toroidal CVT outperforms the full toroidal CVT over the entire operating range in terms of efficiency during ratio variation. These results were predicted in section 5.1 where the link between the traction curve, the optimal ratio variation algorithm and the efficiency was highlighted.

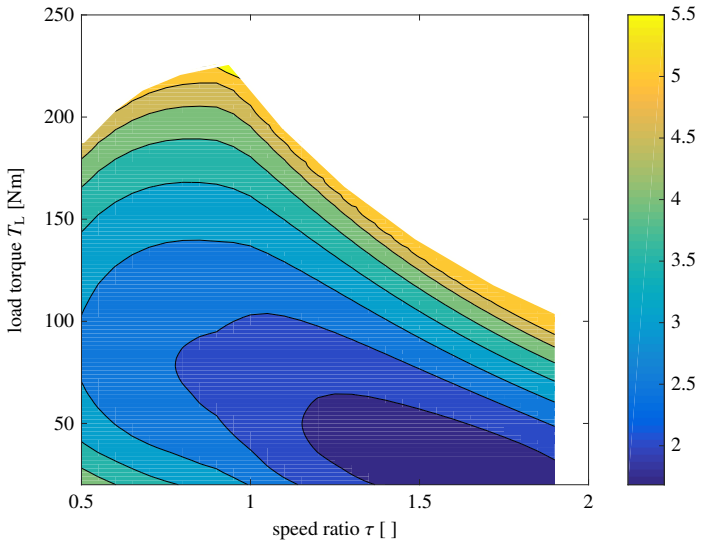

Figure 16: a) Speed ratio τ for the half (blue curve) and full toroidal CVT (red curve). The black line is the speed ratio setpoint. b) Efficiency η during ratio variation for the half (blue curve) and full toroidal CVT (red curve).

8. Design guidelines

Based on the results presented in this paper it is possible to provide the reader with some design guidelines. The goal is to highlight some trends which can be used in the design process of the CVT or bring added value at system level design [42].

In this paper it has been demonstrated that the output torque has a vital impact on the dynamics and that this is independent of the type of topology which is considered. Starting from the equation for the maximum output torque (see eq. (9)), it is possible to identify 3 main contributors to the maximum torque of a toroidal CVT. These are the number of contacts mn, the maximum normal force $F_{\mathrm{N}_{\mathrm{max}}}$ and the maximum friction or traction coefficient $\mu_{\mathrm{out}_{\mathrm{max}}}$. The value r_3 is not considered as this value only identifies the relation between maximum torque and speed ratio and is therefore no parameter which can be optimized in the design stage.

The first term (mn) is related to the units and rollers. This term has a multiplication effect on the output torque which increases the dynamic capabilities but also increases the complexity of the device. Moreover, increasing mn will require more bearings to support the additional rollers and units. This will of course increase the losses of the system but there will also be a cost in terms of material and sizing as the total CVT will become bigger. The bigger size results in another potentially negative side effect: increased inertia. Higher inertia will have, as in any dynamic system, a negative impact on the ratio variation properties. Doubling the output inertia ($J_{\mathrm{out}} = J_{\mathrm{r,out}} + J_{\mathrm{L}}$) will result in a ratio variation period which is two times longer. An important note on that statement is that an increase in the inertia of the output disc $J_{\mathrm{r,out}}$ will only have a significant impact on the dynamics if the inertia of the load J_{L} is of the same order of magnitude.

The second term ($F_{N_{max}}$) is much more interesting to investigate as it is related to the design of the internal components of the CVT. As shown in section 5.2, the maximum normal force is highly dependent on the conformity ratio *CR* which is chosen. Fig. 7 showed that a higher conformity ratio resulted in a higher maximum output torque due to an increased maximum normal force. The side effect of this action was that the maximum efficiency decreased. These relations are now highlighted in Fig. 17 for a wider range of conformity ratio values. The figure confirms the optimal *CR* value of 0.5 in terms of efficiency found by Delkhosh in [28]. On the other hand, the figure also shows that when the conformity ratio is increased towards 0.7, the maximum output torque is doubled while the efficiency decrease is fairly limited. Therefore, the conformity ratio is identified as a very important parameter in terms of the dynamic capabilities of the CVT.

The third and last term ($\mu_{out_{max}}$) is defined by the fluid characteristics of the traction fluid. The importance of the friction coefficient was already briefly mentioned more than a decade ago [43]. It was stated that higher traction coefficients were needed to meet the requirements of automotive transmissions in terms of power and thus torque. In [40] a list of traction fluids is published with their traction characteristics. Other researchers investigated the link between rheological properties and the traction coefficients. In [41, 44] it is shown that there is a positive correlation between the pressure viscosity coefficient and the maximum traction coefficient. Therefore it can be concluded that the pressure viscosity coefficient has an important impact on the maximum friction coefficient.

For dynamic simulations it is not only the maximum friction coefficient which matters, also the gradient towards that maximum value plays its role on the results as elaborated in section 6. This gradient is influenced by spin as shown in section 5.1, which can be limited by high values for the aspect ratio.

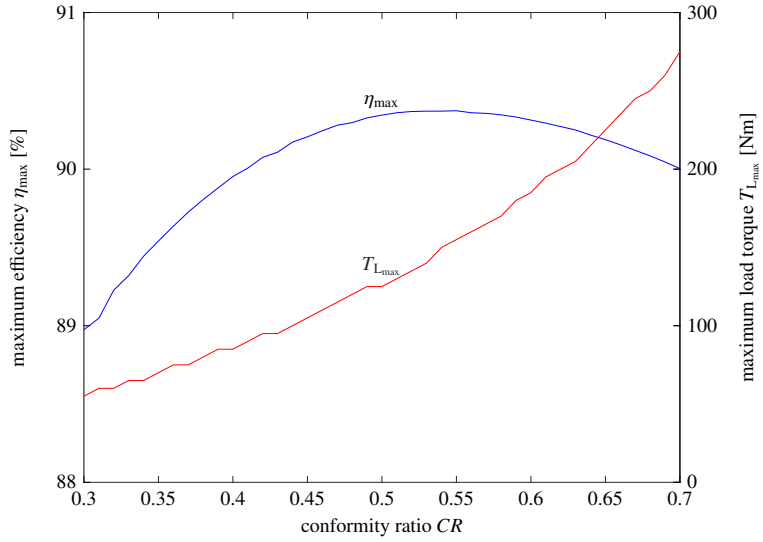

Figure 17: Maximum efficiency η_{max} and maximum load torque $T_{L_{max}}$ for conformity ratio *CR* between 0.3 and 0.7. Speed ratio τ is equal to one and the maximum pressure is kept constant at 2.5GPa.

9. Discussion

In this closing section dynamic results as function of time are shared and their relation with Fig. 13 and Fig. 16 is discussed.

As presented earlier, the difference in dynamic response is summarized in Fig. 13. As validation of this figure, a simulation has been performed in which a series of stepwise speed ratio variations are demanded from both CVTs at a constant load torque of 100Nm (Fig. 18 a)). The step size for these simulations is 0.2.

Fig. 18 a) shows that the difference in ratio variation period between the full and half toroidal CVT is relatively small at low speed ratio values. At higher values, τ equal to 1.3-1.5, the difference suddenly increases much faster. This has been predicted by Fig. 13 where for a load torque of 100Nm no clear variation in difference in speed ratio variation is noticeable until a speed ratio of 1.5.

The reasoning behind this remarkable change can again be explained based on the torque capacity of both topologies. Fig. 10, which displays the torque capacity, shows that from a speed ratio of 1.3 on, the difference in torque capacity grows in favor of the half toroidal CVT. This change has its impact on the dynamics which can be seen in Fig. 13.

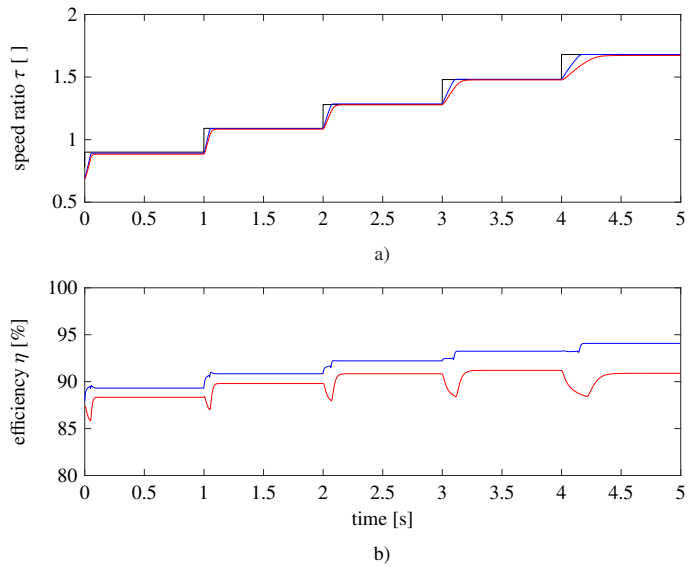

Figure 18: a) Speed ratio variation of the half toroidal (blue curve) and full toroidal (red curve) CVT. The desired speed ratio is given as the black curve. b) Efficiency [%] of the half toroidal (blue curve) and full toroidal (red curve) CVT.

To analyze the difference in efficiency, Fig. 16 is compared with Fig. 18 b). Fig. 16 indicates that significant differences in efficiency will be observed for high speed ratios which is confirmed by 18 b).

Besides the ability to analyze the correctness of Fig. 16, Fig. 18 b) reveals a remarkable trend in the efficiency time series of the half toroidal CVT. It is already proven that the toroidal CVT has a higher efficiency for higher speed ratio [36] but during the transition between speed ratios it is expected to see a drop in efficiency due to the slip which inevitably increases during ratio variation. This phenomenon is clearly visible for the full toroidal CVT but the opposite is true for the half toroidal CVT.

To explain this behavior, the efficiency is split up in a term which considers the torque efficiency η_T (Fig. 19 a)) and a term for the speed efficiency η_ω (Fig. 19 b)) [22].

$$\eta_T = \frac{\mu_{out} - \chi_{out} \sin(\theta - \gamma)}{\mu_{in} + \chi_{in} \sin(\theta + \gamma)} \tag{20}$$

$$\eta_\omega = \frac{\omega_{out} r_3}{\omega_{in} r_1} = 1 - SC \tag{21}$$

What should stand out in Fig. 19 b) is the very high speed efficiency. The reason for the high value is that the pressure in the contacts is controlled and not the slip or speed efficiency. This enabled the authors of this paper to compare the dynamics in a standardized way with fixed torque capacity for both topologies but leads to high speed efficiency values due to too high clamping forces, certainly if the load torque is low.

A consequence of this high speed efficiency or low slip is that the traction coefficient is too low and thus far from ideal. When ratio variation is initiated, slip increases which shortly optimizes the traction conditions leading to a steep increase in torque efficiency. This happens when the speed efficiency drops towards 98%. As the increase in torque efficiency is larger than the decrease of the speed efficiency due to increased slip, the efficiency increases continuously during ratio variation.

This phenomenon can occur at low load torque values for half toroidal CVTs which have a high clamping force to input torque ratio (for safety reasons). This means that even at a low input torque (because the load is relatively small) the clamping force is much more than strictly necessary. In [26], it is shown that this has a negative effect on the steady state efficiency but improves the dynamic response of the CVT.

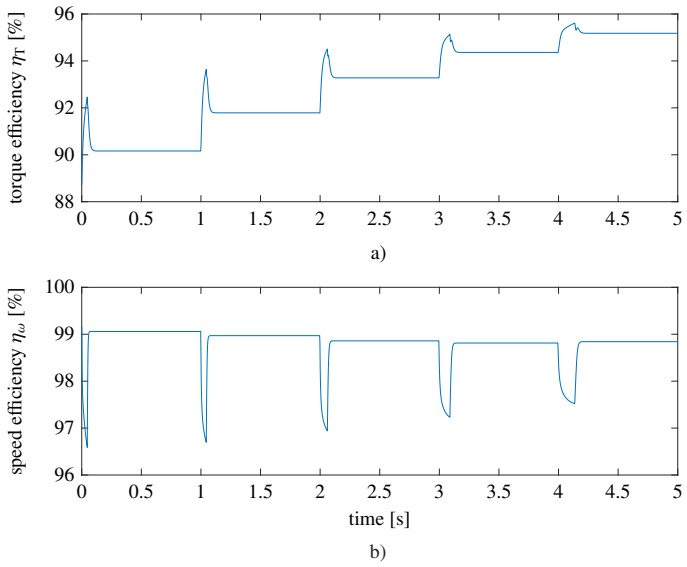

Figure 19: a) Torque efficiency of the half toroidal CVT η_T [%] b) Speed efficiency of the half toroidal CVT η_ω[%]

10. Conclusions

In this paper a comparison is made between the full and half toroidal CVT during dynamic situations. The dynamic response is defined as the period in which the speed ratio is increased by a default value of 0.1. To calculate this quantity, the optimal ratio variation algorithm has been used. Based on that algorithm it is found that the torque capacity of the CVT plays a vital role in the dynamics.

The torque capacity is predominantly defined by the number of contact points, the traction curve and the conformity ratio. The number of contact points can be increased by the number of elements. But this induces problems with sizing and increases losses and complexity of the system. The gradient of the traction curve will play its roll in dynamic situations while the maximum value has its impact on the maximum value of the torque in steady state. The chosen fluid and the amount of spin in the CVT are shown to have a great impact on the traction curve. The conformity ratio, at last, has its impact on torque through the maximum normal force. By varying the conformity ratio it is shown that there is a trade-off between maximum output torque and efficiency. However, this paper proves that the efficiency decrease is negligible compared to the increase in maximum output torque.

The comparison of the dynamic results shows that the half toroidal CVT performs better than the full toroidal CVT over the entire operating range both in terms of dynamics and efficiency. The higher maximum torque at low and high speed ratio values and the much steeper traction curve are the most important reasons for these conclusions. Higher maximum torque results in faster ratio variation and the steeper traction curve induces less slip and thus higher efficiency during ratio variation.

11. Acknowledgments

This research is carried out for the EMTechno project (project ID: IWT150513) supported by VLAIO and Flanders Make, the strategic research center for the manufacturing industry.

12. References

[1] G. Carbone, L. Mangialardi, G. Mantriota, Fuel Consumption of a Mid Class Vehicle with Infinitely Variable Transmission, in: SAE Technical Papers, 2001, pp. 2474–2484. doi:10.4271/2001-01-3692.

[2] F. Van der Sluis, T. Van Dongen, G. J. Van Spijk, A. Van der Velde, A. Van Heeswijk, Fuel consumption potential of the pushbelt CVT, in: Proceedings of FISITA 2006 World Automotive Congress, 2006, pp. 1–12.

[3] L. Mangialardi, G. Mantriota, Dynamic behavior of wind power systems equipped with automatically regulated continuously variable transmission, Renewable Energy 7 (2) (1996) 185–203.

[4] M. L. Shaltout, J. F. Hall, D. Chen, Optimal Control of a Wind Turbine With a Variable Ratio Gearbox for Maximum Energy Capture and Prolonged Gear Life, Journal of Solar Energy Engineering 136 (3). doi:10.1115/1.4026676.

[5] G. C. Tyreas, P. G. Nikolakopoulos, Development and friction estimation of the Half-Toroidal Continuously Variable Transmission: A wind generator application, Simulation Modelling Practice and Theory 66 (2016) 63–80. doi:10.1016/j.simpat.2015.11.007.

[6] S. Akehurst, D. A. Parker, S. Schaaf, Dynamic modeling of the Milner continuously variable transmission - The basic kinematics, Journal of Mechanical Design 129 (11) (2007) 1170–1178. doi:10.1115/1.2771573.

[7] C. Kempermann, Hydrostatic variators for stepless transmissions - Aspects of CVT technology from a supplier's viewpoint, in: VDI-Berichte, 2007, pp. 121–126.

[8] X. Chen, P. Hang, W. Wang, Y. Li, Design and analysis of a novel wheel type continuously variable transmission, Mechanism and Machine Theory 107 (4800) (2017) 13–26. doi:10.1016/j.mechmachtheory.2016.08.012.
URL `http://dx.doi.org/10.1016/j.mechmachtheory.2016.08.012`

[9] G. Carbone, L. Mangialardi, G. Mantriota, The Influence of Pulley Deformations on the Shifting Mechanism of Metal Belt CVT, Journal of Mechanical Design 127 (1) (2005) 103. doi:10.1115/1.1825443.

[10] G. Carbone, L. Mangialardi, B. Bonsen, C. Tursi, P. A. Veenhuizen, CVT dynamics: Theory and experiments, Mechanism and Machine Theory 42 (4) (2007) 409–428. doi:10.1016/j.mechmachtheory.2006.04.012.

[11] N. Srivastava, I. Haque, A review on belt and chain continuously variable transmissions (CVT): Dynamics and control, Mechanism and Machine Theory 44 (1) (2009) 19–41. doi:10.1016/j.mechmachtheory.2008.06.007.

[12] L. Bertini, L. Carmignani, F. Frendo, Analytical model for the power losses in rubber V-belt continuously variable transmission (CVT), Mechanism and Machine Theory 78 (2014) 289–306. doi:10.1016/j.mechmachtheory.2014.03.016.

[13] B. Bonsen, M. Steinbuch, P. a. Veenhuizen, CVT ratio control strategy optimization, in: EEE Vehicle Power and Propulsion Conference, 2005, pp. 227–231. doi:10.1109/VPPC.2005.1554561.

[14] M. a. Kluger, D. M. Long, An Overview of Current Automatic , Manual and Continuously Variable Transmission Efficiencies and Their Projected Future Improvements, in: SAE Technical Papers, 1999, pp. 1–6. doi:1999-01-1259.

[15] T. Imanishi, S. Miyata, Development of the Next-Generation Half-Toroidal CVT, Motion & Control 14 (5) (2003) 20–24.

[16] S. Simons, T. Klaassen, P. Veenhuizen, G. Carbone, Shift dynamics modelling for optimisation of variator slip control in a pushbelt CVT, International Journal of Vehicle Design 48 (1/2) (2008) 45. doi:10.1504/IJVD.2008.021151.

[17] T. Shinojima, T. Toyoda, S. Miyata, T. Imanishi, E. Inoue, H. Machida, Development of the Next-Generation Half-Toroidal CVT with Geared Neutral and Power-Split Systems for 450 Nm Engines, 2004 International Continuously Variable Transmission Congress (2004) 46–54.

[18] A. Brown, J. van Rooij, A. Frank, The design of an inline GCI chain CVT for large vehicles, in: International Continuously Variable and Hybrid Transmission Congress, 2004, pp. 1–15.

[19] E. Solik, A. Frank, P. Erickson, Design improvements on a vee belt CVT and application to a new in-line CVT concept, in: SAE Technical Paper, 2005, pp. 1–9.

[20] Y. Zhang, X. Zhang, W. Tobler, A Systematic Model for the Analysis of Contact, Side Slip and Traction of Toroidal Drives, Journal of Mechanical Design 122 (4) (2000) 523. doi:10.1115/1.1290248.

[21] Z. Zou, Y. Zhang, X. Zhang, W. Tobler, Modeling and Simulation of Traction Drive Dynamics and Control, Journal of Mechanical Design 123 (4) (2001) 556. doi:10.1115/1.1402128.

[22] G. Carbone, L. Mangialardi, G. Mantriota, A comparison of the performances of full and half toroidal traction drives, Mechanism and Machine Theory 39 (9) (2004) 921–942. doi:10.1016/j.mechmachtheory.2004.04.003.

[23] H. Mori, T. Yamazaki, K. Kobayashi, T. Hibi, A study on the layout and ratio change characteristics of a dual-cavity half-toroidal CVT, JSAE Review 22 (3) (2001) 299–303. doi:10.1016/S0389-4304(01)00102-3.

[24] T. Osumi, K. Ueda, H. Nobumoto, M. Sakaki, T. Fukuma, Transient analysis of geared neutral type half-toroidal CVT, JSAE Review 23 (1) (2002) 49–53. doi:10.1016/S0389-4304(01)00149-7.
[25] H. Tanaka, Speed ratio control of a parallel layout double cavity half-toroidal CVT for four-wheel drive, JSAE Review 23 (2) (2002) 213–217. doi:10.1016/S0389-4304(02)00163-7.
[26] F. Verbelen, S. Derammelaere, P. Sergeant, K. Stockman, Half toroidal continuously variable transmission: trade-off between dynamics of ratio variation and efficiency, Mechanism and Machine Theory 107 (2017) 183–196.
[27] T. Imanishi, H. Machida, Development of POWERTOROS Unit Half-Toroidal CVT (2) Comparison between Half-Toroidal and Full-Toroidal CVTs, Motion & Control 10 (1) (2001) 1–8.
[28] M. Delkhosh, M. S. Foumani, Multi-object geometrical optimization of full toroidal CVT, International Journal of Automotive Technology 14 (5) (2013) 707–715. doi:10.1007/s12239.
[29] F. Bottiglione, G. Carbone, L. De Novellis, L. Mangialardi, G. Mantriota, Mechanical hybrid KERS based on toroidal traction drives: An example of smart tribological design to improve terrestrial vehicle performance, Advances in Tribology 2013. doi:10.1155/2013/918387.
[30] H. Tanaka, N. Toyoda, H. Machida, T. Imanishi, Development of a 6 Power-Roller Half-Toroidal CVT, NSK Technical Journal Motion and Control 9 (2000) 15–26.
[31] L. De Novellis, G. Carbone, L. Mangialardi, Traction and Efficiency Performance of the Double Roller Full-Toroidal Variator: A Comparison With Half- and Full-Toroidal Drives, Journal of Mechanical Design 134 (7) (2012) 1–14. doi:10.1115/1.4006791.
[32] A. Yildiz, O. Kopmaz, S. T. Cetin, Dynamic modeling and analysis of a four-bar mechanism coupled with a CVT for obtaining variable input speeds, Journal of Mechanical Science and Technology 29 (3) (2015) 1001–1006. doi:10.1007/s12206-015-0214-y.
URL http://link.springer.com/10.1007/s12206-015-0214-y
[33] Q. Li, H. Li, D. Yu, J. Yao, A novel continuously variable transmission with logarithmic disc generatrix, Mechanism and Machine Theory 93 (24) (2015) 147–162.
[34] S. Miyata, D. Liu, Study of the Control Mechanism of a Half-Toroidal CVT during Load Transmission, Journal of Advanced Mechanical Design, Systems, and Manufacturing 1 (3) (2007) 346–357. doi:10.1299/jamdsm.1.346.
[35] SKF, Rolling bearing catalogue, Tech. rep. (2013).
[36] F. Verbelen, J. Druant, S. Derammelaere, F. De Belie, K. Stockman, P. Sergeant, Benchmarking the permanent magnet electrical variable transmission against the half toroidal continuously variable transmission, Mechanism and Machine Theory 113 (2017) 141–157. doi:10.1016/j.mechmachtheory.2017.03.005.
URL http://dx.doi.org/10.1016/j.mechmachtheory.2017.03.005
[37] J. Tevaarwerk, Johnson, Traction drive performance prediction for the Johnson and Tevaarwerk traction model, in: NASA Technical paper, 1979, pp. 1–39.
[38] Y. Hasuda, R. Fuchs, Development of IVT variator dynamic model, Koyo Engineering Journal English Edition 24 (106E) (2002) 24–28.
[39] R. Fuchs, N. Mccullough, K. Matsumoto, The Making of the Full Toroidal Variator, JTEKT Engineering Journal (1006E) (2009) 31–36.
[40] H. Hata, T. Tsubouchi, Molecular structures of traction fluids in relation to traction properties, Tribol. Lett. 5 (1) (1998) 69–74.
[41] S. Gunsel, S. Korcek, M. Smeeth, H. a. Spikes, The Elastohydrodynamic Friction and Film Forming Properties of Lubricant Base Oils, Tribology Transactions 42 (3) (1999) 559–569. doi:10.1080/10402009908982255.
[42] M. Cammalleri, D. Rotella, Functional design of power-split CVTs: An uncoupled hierarchical optimized model, Mechanism and Machine Theory 116 (2017) 294–309. doi:10.1016/j.mechmachtheory.2017.06.003.
[43] S. C. Tung, M. L. McMillan, Automotive tribology overview of current advances and challenges for the future, Tribology International 37 (7) (2004) 517–536. doi:10.1016/j.triboint.2004.01.013.
[44] T. Zolper, Z. Li, M. Jungk, A. Stammer, H. Stoegbauer, T. Marks, Y. W. Chung, Q. Wang, Traction characteristics of siloxanes with aryl and cyclohexyl branches, Tribology Letters 49 (2) (2013) 301–311. doi:10.1007/s11249-012-0066-x.